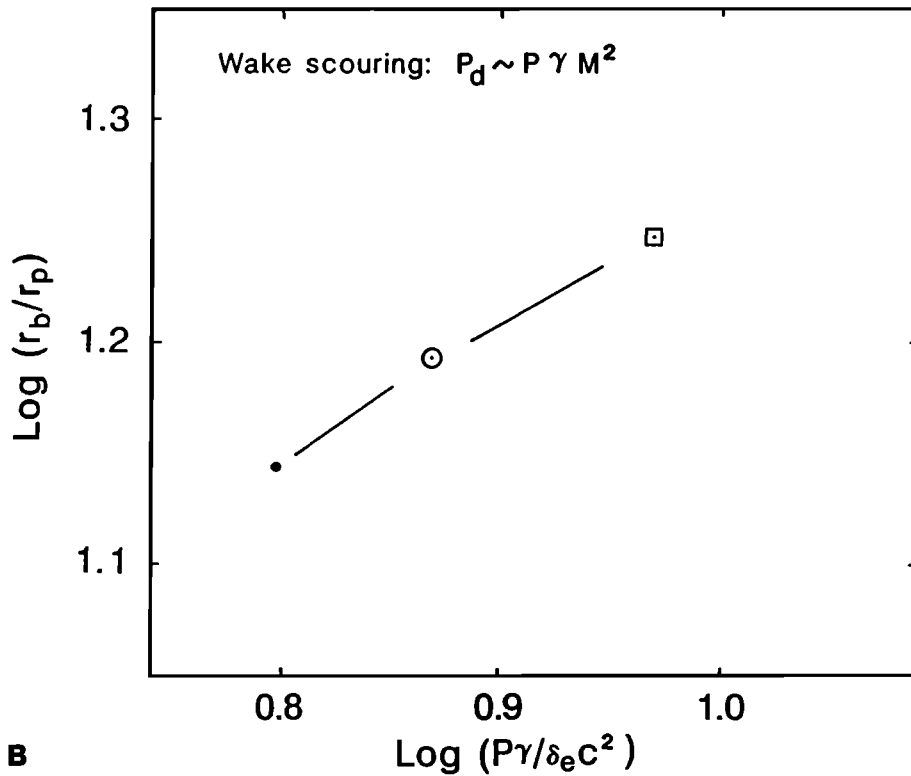


A



B

Fig. 13. Wake-blast scouring efficiency expressed in terms of a subsonic wind (Figure 13a) and supersonic blast (Figure 13b). Figure 13a relates the observed radius  $r_b$  of the wake-blast scaled to impactor radius  $r_p$  (more specifically, square root of the sand-scoured area to projectile cross-sectional area) to the impinging dynamic pressure ( $\rho v^2$ ) of a subsonic wake wind where it is assumed that the impact velocity of the wake wind is a constant fraction of the impactor velocity. The size of the wake-blast zone gradually increases with dynamic pressure at low impact velocities but is increasingly enhanced at high velocities. Figure 13b considers the wake blast size for only hypervelocity impactors

expressed in terms of the stagnation pressure  $P_s$  of the colliding wake of incompressible gas ( $P_s = P\gamma M^2$ , for pressure  $P$ , ratio of specific heat  $\gamma$ , and Mach number  $M$ ). When  $P\gamma M^2$  is scaled to  $\delta_e v_i^2$ , the resulting dimensionless ratio becomes  $(P\gamma/\delta_e c^2)$ , which depends simply on  $(P\gamma/c^2)$  for a given target. Figure 13, then, provides evidence that the colliding wake decoupled from the projectile might affect crater scaling, particularly at high Mach numbers and high atmospheric densities. (Density  $\rho$  is shown in terms of ambient air, sand density is assumed to be unity;  $P$  is in bars with  $v$  and  $c$  in km/s.)